Effect of Chemical Lithium Insertion into Rutile TiO2 Nanorods

ARTICLE · JANUARY 2009

9 AUTHORS, INCLUDING:

Murugesan Vijayakumar
Pacific Northwest National Laboratory
87 PUBLICATIONS **1,028** CITATIONS
SEE PROFILE

Kevin M. Rosso
Pacific Northwest National Laboratory
180 PUBLICATIONS **4,718** CITATIONS
SEE PROFILE

Effect of Chemical Lithium Insertion into Rutile TiO_2 Nanorods

M. Vijayakumar, Sebastien Kerisit, Chongmin Wang, Zimin Nie, Kevin M. Rosso, Zhenguo Yang, Gordon Graff, Jun Liu, and Jianzhi Hu*

Pacific Northwest National Laboratory, Richland, Washington 99352

Received: May 4, 2009; Revised Manuscript Received: June 11, 2009

Rutile TiO_2 nanorods were synthesized by hydrolysis of $TiCl_4$ followed by a hydrothermal method. Lithium insertion into the rutile nanorods was achieved by a chemical lithium insertion process. The structural evolution of nanostructured rutile upon lithium insertion was characterized by several experimental techniques, namely, XRD, TEM, SAED and ^{6}Li MAS NMR. The XRD and TEM studies indicate the formation of lithium titanate phase (Li_xTiO_2) during lithium insertion. Additionally, SAED patterns show that the lithium titanate phase has cubic symmetry. Finally, high magnetic field (21.1 T) ^{6}Li MAS NMR reveals that the lithium titanate phase adopts two different structures depending on lithium content. Taken together, the four techniques consistently show that the insertion of lithium into rutile TiO_2 nanorods causes two consecutive structural phase transformations to lithium titanate phases with spinel ($Fd\bar{3}m$) and rocksalt ($Fm\bar{3}m$) structures at $x = 0.46$ and 0.88, respectively. In addition, the broad line widths in the ^{6}Li MAS NMR spectrum of the rocksalt phase are indicative of a disordered structure. Density functional theory calculations of the rutile, spinel and rocksalt bulk phases as a function of lithium content corroborate the observed phase transformations. These phase transitions could account for the irreversible capacity loss of nanostructured rutile anodes observed in electrochemical cycling experiments.

Introduction

Over the past decade, a tremendous amount of research has contributed to the search for better electrode materials for lithium ion batteries.[1] In particular, transition metal oxides with tunnel or framework structures have been widely investigated as electrode materials.[2] Among the various transition metal oxides, titanium dioxide (TiO_2) is an excellent candidate for anode material due to its low production cost, low environmental impact, and high capacity.[3] The three common TiO_2 polymorphs, namely, anatase ($I4_1/amd$), rutile ($P4_2/mnm$), and brookite ($Pbca$), have been tested as anode materials but showed limited success in their bulk form.[4] Recent developments in the area of nanostructured transition metal oxides led to reinvestigation of the TiO_2 polymorphs as anode materials.[5,6] For instance, nanostructured anatase showed excellent improvement in rate capacity over bulk anatase.[7] In particular, the extent of lithium insertion into anatase improved dramatically with crystallites of decreasing size and resulted in the extension of solid solution domains.[8] Similarly, rutile TiO_2, once considered electrochemically inactive at room temperature in micrometer-sized form,[9] shows high capacity and better lithium electrochemical activity in its nanostructured form.[10] These surprising advantages of nanosized TiO_2 compared with micrometer-sized TiO_2 stimulated further research in TiO_2 nanostructures. In particular, various nanostructured morphologies such as nanoparticles,[11] nanorods,[7] nanotubes[12] and nanowires[13] of TiO_2 have been tested as anode material with promising results. However, in spite of its high capacity, nanostructured rutile TiO_2 has shown a high degree of irreversibility, which degrades the battery performance after a few cycles.[10,14] The occurrence of a structural phase transition during lithium insertion is believed to be the reason for this capacity loss with electrochemical cycles.[15] The occurrence of a phase transformation during lithiation of rutile TiO_2 was corroborated by the constant potential plateaus observed during slow galvanostatic extraction of lithium ions.[9]

This phase transformation during lithium insertion directly affects the efficiency of the battery and raises new questions about the nature of the lithium interaction with the TiO_2 host structure. Various experimental[16−18] and theoretical[19−21] studies have revealed that lithium insertion into both rutile and anatase TiO_2 leads to a lithium titanate (Li_xTiO_2) phase, which has many polymorphs with hexagonal ($R\bar{3}m$), cubic spinel ($Fd\bar{3}m$), monoclinic ($P2/m$) and cubic rocksalt ($Fm\bar{3}m$) symmetries. Despite numerous reports, the exact nature of lithium insertion and structural information about lithium titanate phase are still not well understood. For instance, there is still ambiguity about the nature of the structural changes in nanostructured rutile upon lithium insertion. Baudrin et al.[22] reported that complete lithium insertion (i.e., $x = 1$) into the nanostructured rutile resulted in the formation of lithium titanate phase with the rocksalt structure. However, Koudriachova et al.[23] predicted, using first-principles calculations, the formation of the hexagonal structure upon lithium insertion into rutile TiO_2. Finally, Borghols et al.[15] reported that, for a lithium concentration of $x = 0.85$, rutile structure transforms to a monoclinic structure closely resembling the hexagonal structure. In addition to these final phases, intermediate phases are also expected to occur during lithium insertion. For example, the electrochemical experiment of rutile TiO_2 shows a plateau region at 1.4 V which indicates a possible phase transition at x in the range of 0.5 (i.e., $Li_{0.5}TiO_2$). Two possible structures have been reported for this $Li_{0.5}TiO_2$ phase: a slightly distorted monoclinic ($P2/m$) structure[15] and a cubic spinel structure.[24] In conclusion, further studies are needed for a better understanding of the formation and structural evolution of lithium titanate during lithium insertion into nanostructured TiO_2.

* Corresponding author. E-mail: Jianzhi.Hu@pnl.gov. Phone: (509) 371-6544. Fax: (509) 371-6546.

10.1021/jp904148z CCC: $40.75
Published on Web 07/02/2009

TABLE 1: Lithium Concentration, Particle Size and ^{6}Li NMR Parameters of Lithium Inserted Rutile TiO_2 Nanorod

				^{6}Li NMR parameters			
sample	phase	structure[a]	av particle size[b] (nm)	δ_{iso} (ppm) $\pm$ 0.05	$\Delta\nu$ (Hz)	T_1 (s)	integral ratio (%)
R1	$Li_{0.10}TiO_2$	rutile ($P4_2/mnm$)	70 nm	0	27	64 ± 4	100
R2	$Li_{0.12}TiO_2$	rutile ($P4_2/mnm$)	70 nm	0	33	72 ± 5	21
	$Li_{0.46}TiO_2$	cubic spinel ($Fd\bar{3}m$)	90 nm	0.41	125	82 ± 9	79
R3	$Li_{0.12}TiO_2$	$P4_2/mnm$ (rutile)	70 nm	0	35	75 ± 5	12
	$Li_{0.88}TiO_2$	cubic rocksalt ($Fm\bar{3}m$)	100 nm	-0.34	170	135 ± 10	88

[a] Structure based on SAED pattern and ^{6}Li NMR spectra (see text for details). [b] Average particle size measured from TEM measurement; in case of nanorod rutile particles the size represents average width of the rod (see text for details).

To clarify the structural evolution of nanostructured rutile upon lithiation, in this work nuclear magnetic resonance (NMR) spectroscopy, X-ray diffraction (XRD), transmission electron microscopy (TEM), and density functional theory (DFT) were used to study the chemically inserted rutile nanorods. The use of ^{6}Li solid state NMR to study lithium inserted metal oxides has been recently reported and proven to be a sensitive tool for structural studies.[25] Lithium inserted TiO_2 has previously been studied by ^{6}Li MAS NMR,[26,27] however the data in these studies were acquired at low magnetic fields ($\leq$11.7 T), and hence suffered from poor spectral resolution. In the present work, ^{6}Li MAS NMR studies were carried out under high magnetic field (21.1 T) to explore the local structural information of lithium inserted rutile TiO_2. The experimental NMR data are compared with results from electronic structure calculations and the possible phase transformations upon lithium insertion are discussed.

Experimental Details

Rutile TiO_2 nanorods were prepared by hydrolysis of $TiCl_4$ followed by hydrothermal treatment method. In a typical synthesis, 2 mL of titanium tetrachloride was added dropwise into 20 mL of ice water under vigorous stirring until the white fog disappeared. After stirring, the solution was heat treated at 65 °C for 2 h to facilitate the hydrolysis reaction. The solution was then transferred to a Teflon coated autoclave vessel and heat treated at 120 °C for 12 h. After the hydrothermal treatment, the sample was washed with water and dried in an oven at 100 °C for 2 h. The resulting sample has nanorod-type morphology and was found to be in pure rutile phase (sample R). Lithium insertion into these rutile nanorods was done by a hydrothermal reaction. Each sample was prepared by mixing 0.4 g of rutile nanorods, 20 mL of deionized water, and a varying amount of LiOH depending on the target stoichiometry. The samples were stirred at room temperature for 6 h and then heat treated in the Teflon coated autoclave vessel at 180 °C for 12 h to facilitate the hydrothermal reaction. Then the products were filtered and rinsed with copious amounts of water to remove any unreacted LiOH and dried at 100 °C for 2 h. The amounts of LiOH were chosen to achieve Li/Ti ratios of 0.5, 1 and 2, and the three resulting samples were labeled R1, R2 and R3, respectively. The products were identified by X-ray powder diffractometry (XRD) using a Philips Xpert X-ray diffractometer using Cu Kα radiation at $\lambda \sim 1.54$ Å. The particle size and shape were analyzed with a JEOL-JSM2010 tunneling electron microscope (TEM) operated at 200 kV.

^{6}Li NMR measurements were made using a Varian 900 Inova magnet ($B_0 = 21.1$ T and ^{6}Li Larmor frequency of 113.56 MHz) with magic angle spinning (MAS) at 10 kHz using 3.2 mm zirconia rotors and a homemade pencil-type MAS probe. Chemical shifts were referenced to solid LiCl samples ($\delta_{iso} = -1.26$ ppm with respect to 1 M LiCl solution $\delta_{iso} = 0$ ppm) at spinning speeds of 10 kHz. The estimated uncertainty in chemical shifts was 0.05 ppm, and was determined through calibration using the same reference sample. The lithium spin concentration measurements were done using ^{7}Li MAS NMR on a Chemagnetics 300 spectrometer ($B_0 = 7.1$ T, MAS = 5 kHz and ^{7}Li Larmor frequency of 116.53 MHz) in which the intensities of all the samples were compared with standard lithium compounds, i.e., Li_2TiO_3 and Li_2CO_3 obtained from Aldrich. To obtain quantitative results, the whole spectra of standard lithium compounds were deconvoluted, including the side bands, and the area under each peak was scaled to the known lithium concentration. Similarly, the spectra of the lithium inserted samples were deconvoluted, including the side bands, and the area under each peak was compared with that of the Li_2TiO_3 standard to determine the lithium concentration in each TiO_2 sample (R1, R2 and R3). For the mixed phase compounds (R2 and R3), the lithium concentration in each phase was derived from the ratio of deconvoluted peaks and their respective ^{6}Li MAS NMR spectra. Accurate intensities of the contributions were obtained from fitting the line shapes of the resonance lines with a mix of a Gaussian and Lorentzian line shapes using the DMFIT program.[28] The estimated uncertainty in these spin concentration measurements was $\pm$0.04 and determined through a trial and error method in deconvolution of spectra. Lithium concentrations for each sample along with NMR parameters are shown in Table 1. Spin$-$lattice relaxation (T_1) measurements were carried out using a saturation recovery method under magic angle spinning. All lithium samples were heat treated at 100 °C for 2 h before packing in NMR rotors to remove any surface adsorbed water.

Computational Methods

Ab initio energy minimizations of titania polymorphs with varying lithium contents were carried out using CRYSTAL06.[29] CRYSTAL06 makes use of the linear combination of atomic orbitals (LCAO) approach whereby the crystalline orbitals are constructed from a linear combination of space-symmetry-adapted Bloch functions defined in terms of local Gaussian functions. In all calculations a full optimization of the atomic coordinates and the cell parameters was carried out using spin unrestricted density functional theory (DFT) and the B3LYP exchange-correlation potential. One important point to note in these periodic calculations is that basis sets must be chosen to avoid overly diffuse functions and quasi-linear dependence of the Bloch functions. Therefore, the basis-set exponents and coefficients were first optimized at the B3LYP level with LOptCG[30] for experimentally derived structures. The Ti and O basis sets were optimized using the TiO_2 rutile structure with the Durand-21d41 electron core pseudopotential (ECP) basis set of Catti et al.[31] and the Durand-41 ECP basis set of Apra[32] as starting points for Ti and O, respectively. Both basis sets use the electron core pseudopotential of Durand and Barthélat,[33]

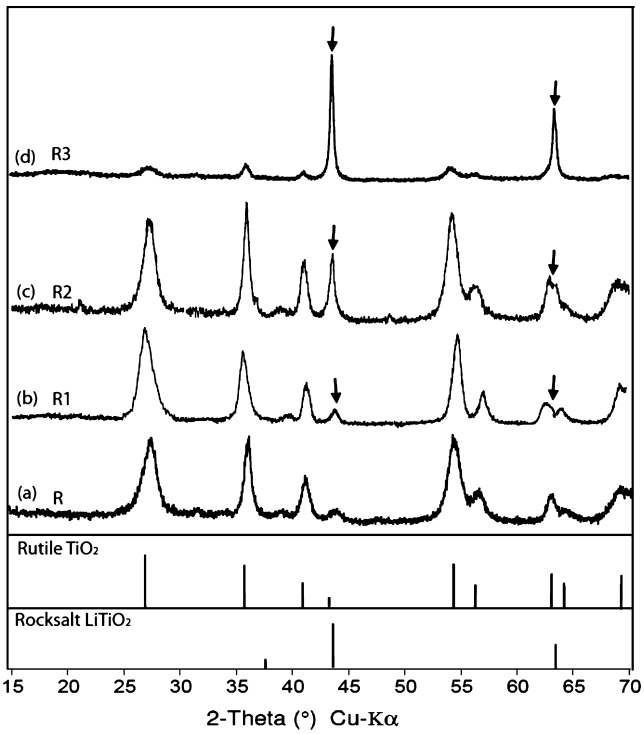

Figure 1. X-ray diffraction patterns of as-prepared TiO_2 sample R (a) and lithium inserted rutile TiO_2 nanorod samples (b, c and d) where (b) is sample R1 (i.e., initial Li/Ti = 0.5), (c) sample R2 (i.e., initial Li/Ti = 1), and (d) sample R3 (i.e., initial Li/Ti = 2). Arrows indicate lithium titanate phase and vertical lines show rutile ($P4_2/mnm$) and cubic rocksalt ($Fm\bar{3}m$) diffraction patterns from JCPDS 021-1276 and 16-0223, respectively.

i.e., for Ti only the 4s, 4p, and 3d orbitals are treated explicitly and for O only the 3s and 2p orbitals are treated explicitly. The Li basis set was optimized with the Li_2O structure[34] and the all-electron 6-11G basis set of Dovesi et al.[35] as starting point together with an 8-411 all-electron basis set for O. The final Li basis set was a 6-1G construction.

Based on our experimental results described below, three titania polymorphs were considered, namely, the rutile,[36] spinel,[37] and rocksalt[38] structures. For the rutile and rocksalt structures, a $2 \times 2 \times 2$ supercell was employed whereas a $1 \times 1 \times 1$ cell was sufficient for the spinel structure. All three simulation cells contained 16 TiO_2 units. Five different Li contents, Li_xTiO_2, were considered, namely, 0.00, 0.25, 0.50, 0.75, and 1.00, which correspond to 0, 4, 8, 12, and 16 Li atoms in the supercells, respectively. For rutile, the Li ions were initially inserted in the octahedral sites in the *c*-direction channels. An ordered configuration of the rocksalt structure was considered whereby the crystal is composed of alternating TiO_2 and LiO_2 layers for $x = 1$, and LiO_2 layers are depleted in Li at lower Li contents. In the spinel structure, the Li ions can occupy both the tetrahedral and octahedral sites depending on the Li content. Upon lithium intercalation, a charge compensating electron must also be present; for example, Ti^{4+} nominally becomes Ti^{3+} with an unpaired electron. As only even numbers of lithium ions were inserted, we selected antiparallel coupling of unpaired spins to produce calculations that have a net spin of zero in every case.

Results and Discussion

XRD. Figure 1 shows the XRD patterns of as-prepared (sample R) and chemically lithium inserted (samples R1, R2, and R3) TiO_2 samples. The XRD pattern of the as-prepared TiO_2 particles (Figure 1a) shows the formation of pure rutile phase TiO_2 [JCPDS 021-1276]. The broad nature of the Bragg peaks indicates the formation of a nanostructured material. Similarly, the lithium inserted sample R1 also shows only rutile diffraction patterns (Figure 1b) indicating that the material is initially retaining a rutile-type structure upon lithiation. Further lithium insertion (samples R2 and R3) leads to the appearance of new peaks ($2\theta = 43.8$ and 63.5°) indicating the formation of lithium titanate (Figures 1c and 1d). The relative amount of the rutile and lithium titanate phases in each sample is linearly proportional to the amount of lithium inserted. For sample R3 (i.e., Li inserted with Li/Ti ratio of 2), nearly 90% of the parent rutile has undergone phase transformation to the lithium titanate structure (see Figure 1d). It is interesting to note that the Bragg peaks of the lithium titanate phase in the powder XRD pattern are sharper compared to those of the parent rutile phase peaks. This suggests that the lithium titanate phase consists of crystallites of slightly increased size and is possibly more crystalline. However, no significant line broadening is observed in the Bragg peaks of the parent rutile phase due to lithium insertion. This indicates that there is no phase coexistence (domains having a different crystal phase) and each crystallite particle in the lithiated samples is either converted completely to the lithium titanate phase or retains the parent rutile structure. The Bragg peaks ($2\theta = 43.8$ and 63.5°) of lithium titanate match those reported in the literature for disordered rocksalt lithium titanate [JCPDS 16-0223, $Fm\bar{3}m$; $a = 4.126$ Å].[38] However, these lines can also be indexed with hexagonal and spinel structures, making it difficult to precisely define the structure of the lithium titanate phase based solely on such broad lines with possible overlaps.

TEM. Figure 2 shows typical transmission electron microscopy (TEM) images of as-prepared and lithium inserted TiO_2 samples. The as-prepared TiO_2 samples show (Figure 2a) composite aggregates consisting of straight and well-defined nanowires. The nanowires are several hundred nanometers long and have a width of about 10 nm. However, severe agglomeration of these nanowires results in rodlike features with average width of 70 nm (see Figure 2a). Due to this severe agglomeration, these rutile TiO_2 nanowires will be considered to have nanorod-like structures hereafter. Selected area electron diffraction (SAED) patterns (inset in Figure 2a) on these nanorods reveal a crystalline rutile phase. The SAED patterns also show a pair of strong (110) reflections, indicating that the (110) planes of the rutile nanocrystals are locally preferably oriented. Similarly, the lithium inserted sample R1 shows a rutile structure in the SAED patterns (inset in Figure 2b) and also retains the same rodlike morphology with similar size and shape (see Figure 2b). Further lithiated sample R2 (Figure 2c) shows the presence of rectangular particles along with rodlike rutile particles. On the other hand, the high lithium inserted sample R3 shows (Figure 2d) mostly rectangular-like crystalline particles with parent TiO_2 nanorods scarcely observed. Based on the X-ray diffraction patterns (Figures 1c and 1d) of samples R2 and R3, which show a mixture of rutile and lithium titanate phases, we deduce that the rectangular-like crystalline particles are lithium titanate particles. It is interesting to note that the lithium titanate crystallites in both samples R2 and R3 show similar rectangular-like morphologies with only slight differences in their sizes (see Figure 2c and 2d). To help identify the structure of the lithium titanate phase, SAED was taken on the rectangular crystalline particles. The SAED pattern for sample R2 (inset in Figure 2c) on the rectangular particles shows a set of diffraction rings along the [100] zone axis, which are labeled as (220), (440) and (400) and represent a spinel structure

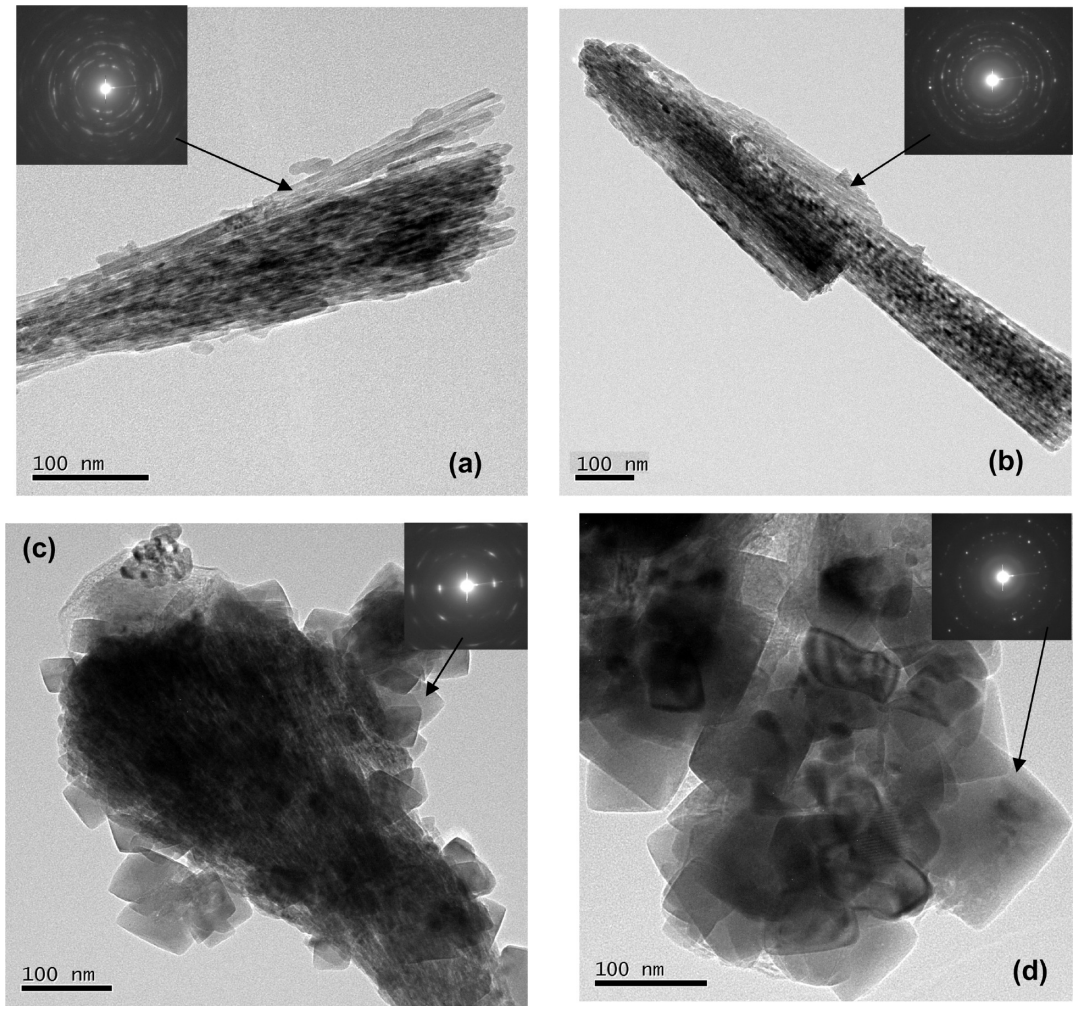

Figure 2. TEM images of as-prepared rutile TiO_2 nanorods (a) and lithium inserted rutile TiO_2 nanorods (b, c, and d) where (b) is sample R1, (c) sample R2, and (d) sample R3. Insets in images show the corresponding SAED patterns of particles indicated by arrow.

($Fd\bar{3}m$; $a = 8.402$ Å).[39] Similarly, in the SAED pattern along the [001] zone axis for sample R3 (inset in Figure 2d), the main diffraction rings are assigned to the (200), (220), and (222) reflections of the rocksalt lithium titanate phase ($Fm\bar{3}m$; $a = 4.126$ Å).[40] These results suggest that the lithium titanate particles exist mainly in a cubic phase and that there is no hexagonal or monoclinic phase of lithium titanate present. Whether a spinel or rocksalt lithium titanate phase is formed depends primarily on the amount of lithium inserted into the parent rutile nanorods. The TEM images also revealed that, during chemical lithium insertion, the rutile nanorods broke into rectangular-like lithium titanate crystallites. Our previous report of electrochemical lithium insertion in nanostructured rutile shows the overall morphology is retained even after a phase transition.[40] Hu et al.[10] reported the formation of smaller crystallite grains during electrochemical lithium insertion in nanostructured rutile, however the overall shape of initial particles is preserved during electrochemical cycling. In the present study, the formation of new crystallites is predominant with chemical lithium insertion. The phase transition due to lithium insertion accompanied with prolonged heat treatment (see Experimental Details) could cause the nucleation of these new crystallites with lithium titanate phase. From these TEM results, it is clear that lithium insertion into rutile nanorods induces structural transformation into either a spinel or rocksalt type lithium titanate phase. However, one needs a more sensitive local probe to understand the structural transformation and ^{6}Li MAS NMR is an excellent tool to get more insight into the local structure of lithium titanate phases.

^{6}Li MAS NMR. The quadrupolar moment of ^{6}Li (-8×10^{24} Q/m^2) is one fiftieth of that of ^{7}Li (-4×10^{26} Q/m^2), Larmor frequency of ^{6}Li is about 2.6 times smaller than that of ^{7}Li and its natural abundance is only about 7%. For these reasons homonuclear dipole−dipole interactions and quadrupolar broadening are much weaker, hence ^{6}Li MAS NMR offers better spectral resolution than traditional ^{7}Li MAS NMR. Figure 3a shows the ^{6}Li MAS NMR spectra of lithium inserted nanostructured rutile TiO_2 under a 21.1 T magnetic field with spinning speed of 10 kHz. The sample R1 shows a single sharp resonance (peak A) at about 0.03 ppm with a line width ($\Delta\nu$) of about 20 Hz. Figure 3b shows the observed and deconvoluted ^{6}Li spectra for sample R2 (bottom) and R3 (top). The samples with high lithium concentrations (samples R2 and R3) show broad overlapping resonance (peak B or peak C) along with a sharp resonance (peak A). The contribution of the narrow resonance (peak A) to the total spectra decreases with increasing lithium concentration. From the XRD results, we know that the proportion of the parent rutile phase is decreasing with increasing lithium concentration (Figure 1). Integrating these results, the sharp resonance (peak A) can be assigned to lithium ions in rutile and the broad resonances to lithium in the titanate phase. Because the NMR measurements are performed quantitatively,

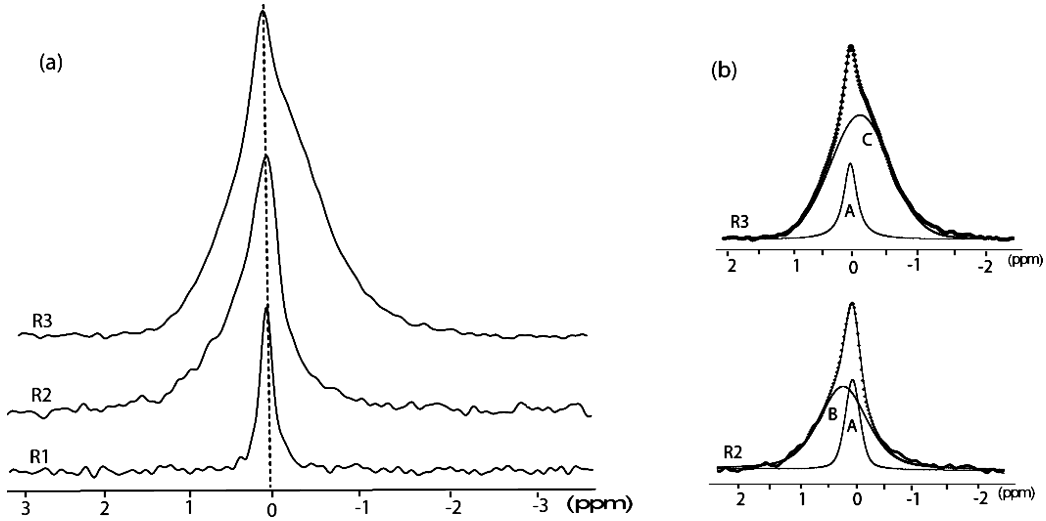

Figure 3. (a) ^{6}Li MAS NMR spectra measured at 21.1 T with spinning frequency of 10 kHz for lithium inserted rutile nanorods. (b) Deconvoluted spectrum of sample R2 (bottom) and sample R3 (top). The dotted lines represent the experimental spectrum, and solid lines are the fitted Gaussian/Lorentzian line shape.

the ratio of the integrated signal of the broad and sharp resonances equals the ratio of the amount of lithium in both environments. For these quantitative results the whole spectra have been deconvoluted and the relative amount of lithium in each environment is derived from the ratio of two resonance spectra. As the overall lithium compositions are already determined from the spin concentration measurements using ^{7}Li MAS NMR, the absolute amount of lithium in each phase can be calculated from the ^{6}Li peak area. The lithium compositions for all the samples with their phase are tabulated in Table 1.

From the spin concentration measurements, the lithium concentration in sample R1 was found to be $Li_{0.10}TiO_2$. Sample R1 shows a single sharp resonance (peak A) which indicates lithium occupies only one crystallographic site inside the rutile structure and has a highly uniform coordination as expected for the highly ordered rutile structure. As a spin $I = 1$ nuclei, ^{6}Li has no isotropic first-order quadrupolar shift and the second-order quadrupolar shift is negligible due to its extremely small quadrupolar moment[41] and the high magnetic field (21.1 T) used in the present study. Thus the observed peak center for ^{6}Li MAS spectrum is very close to the isotropic chemical shift (δ_{iso}) of ^{6}Li. Xu et al. reported the correlation between ^{6}Li chemical shifts (δ_{iso}) and lithium coordination for diamagnetic crystalline and glassy silicates.[42] In these materials, the high lithium coordination resonances are shifted toward negative chemical shifts due to higher chemical shielding. For example, lithium in 6-fold coordination (LiO_6) has a chemical shift around -1 ppm whereas lithium in 4-fold coordination (LiO_4) shows peak around $+1$ ppm. On the basis of this report, the ^{6}Li peak position of sample $Li_{0.12}TiO_2$ is an indication of the oxygen coordination and thus to the position of lithium in the rutile lattice. The rutile structure consists of TiO_6 polyhedra that share edges in the *c* direction and corners in the *ab* planes (Figure 4a). This packing result in two possible sites for lithium insertion, a tetrahedral site, which is formed by the edge-sharing TiO_6 octahedra along the *c* direction, and a octahedral site, formed by the corner-sharing TiO_6 octahedra along the *ab* planes. A recent density functional theory study showed the octahedral site is energetically favored over the tetrahedral site for lithium insertion.[43] According to lithium chemical shift correlation data,[42,44] for the LiO_6 polyhedra, the peak position is expected to be around -1 ppm, but our spectrum shows a peak positioned at 0.03 ppm. This is surprising since ^{6}Li MAS NMR suggests lithium

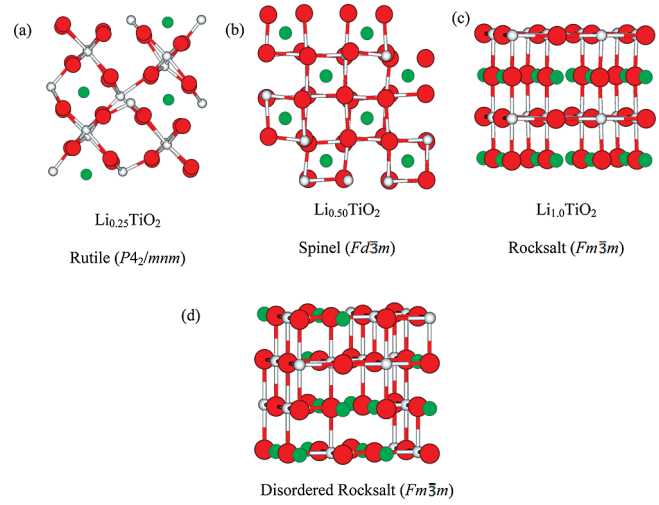

Figure 4. Illustration of different crystal structures observed during lithium insertion in rutile TiO_2 nanorods. The structures used in DFT study are shown in panels a−c: (a) lithium inserted tetragonal rutile ($P4_2/mnm$) structure; (b) spinel ($Fd\bar{3}m$) lithium titanate phase; (c) ordered rocksalt ($Fm\bar{3}m$) lithium titanate phase. Panel d shows illustration of possible cation distribution resulting in disordered rocksalt type structure as predicted from ^{6}Li MAS NMR result (see text for details).

effective coordination is less than six in the rutile nanorods. This can be explained with the possibility of lithium being in an off-center position inside the octahedral site, which could reduce the Li−O bond lengths and hence effectively reduce the lithium coordination. This is consistent with DFT calculations reported by Koudriachova et al.[45] This type of Li off-center position has been observed in Li-ramsdellite structure[46] and anatase structure by neutron diffraction data and theoretical studies.[47] Hence, from the ^{6}Li resonance we can infer that lithium is being accommodated in an off-centered octahedral position during lithiation of the rutile structure.

The ^{6}Li MAS NMR spectrum (Figure 3b) of further lithiated TiO_2 (sample R2) shows two overlapping peaks, a sharp resonance at 0.01 ppm (peak A) and a broad resonance at 0.41 ppm (peak B). This result is consistent with XRD (Figure 1c) where the presence of both the rutile and lithium titanate phases was detected. The sharp resonance (peak A) has already been assigned to lithium in rutile, therefore the broad resonance (peak

B) must represent lithium in lithium titanate. From lithium spin concentration measurements the lithium concentration in the rutile and lithium titanate phases was found to be $Li_{0.12}TiO_2$ and $Li_{0.46}TiO_2$, respectively. The chemical shift of broad peak B ($\delta_{iso} = 0.41$ ppm; $\Delta\nu \approx 125$ Hz) suggests lithium occupies a site with tetrahedral coordination in the lithium titanate ($Li_{0.46}TiO_2$) phase. Lithium titanate (Li_xTiO_2) reportedly has many polymorphs, including cubic spinel, hexagonal, and cubic rocksalt type structure. The spinel Li_xTiO_2 ($x \leq 0.5$) is the only polymorph of lithium titanate where Li^+ ions are known to have tetrahedral co-ordination.[24] Hence the resonance at 0.4 ppm (peak B) for sample R2 (Figure 3b) can be assigned to lithium in spinel type Li_xTiO_2. This result agrees with SAED pattern (inset in Figure 2c) where the lithium titanate phase ($Li_{0.46}TiO_2$) of sample R2 was identified as having the spinel structure.

The ^{6}Li MAS NMR spectrum of sample R3 (Figure 3b) shows two overlapping resonances, a sharp resonance at 0.01 ppm (peak A) and a broad resonance at -0.34 ppm (peak C). The sharp resonance (peak A) is similar to other lithiated samples, indicating lithium in rutile phase and the broad resonance (peak C) represents lithium titanate phase. The intensity of sharp resonance is greatly reduced revealing that most of the rutile structure has been phase transformed to lithium titanate structure, which is consistent with our XRD results (Figure 1d). From lithium spin concentration measurements the lithium concentration in lithium titanate phase is $Li_{0.88}TiO_2$ (peak C) and rutile phase is $Li_{0.12}TiO_2$ (peak A). It is noteworthy that even under overloading of LiOH (i.e., Li/Ti ratio of 2) during hydrothermal treatment, the maximum lithium upload is 0.12Li/Ti, which is lower than the theoretical capacity of rutile (1.0Li/TiO_2), but still quite large compared with bulk rutile (0.03Li/Ti) as discussed in the Introduction. This upper limitation of lithium insertion could depend on the particle size of initial rutile particles, so further reduction in the particle size might help to achieve the theoretical capacity.[8] The chemical shift of $Li_{0.88}TiO_2$ (peak C at -0.34 ppm; $\Delta\nu \approx 170$ Hz) is significantly different from chemical shift of $Li_{0.46}TiO_2$ (peak B at 0.41 ppm). Clearly, lithium in sample R3 ($Li_{0.88}TiO_2$) has a different environment than in sample R2 ($Li_{0.46}TiO_2$). The relatively high shielding (lower chemical shift) of $Li_{0.88}TiO_2$ suggests lithium resides in an octahedral environment. The spinel structure holds lithium in tetrahedral sites; however, for lithium concentrations greater than 0.5, lithium starts occupying the vacant octahedral sites (16*c*) along with regular tetrahedral sites (8*a*).[24] Hence, two ^{6}Li MAS NMR resonances (from lithium in the octahedral and tetrahedral sites) are expected for spinel samples with $x \geq 0.5$, but the spectrum in Figure 3b shows only one resonance (peak C) indicating that lithium is present in an octahedral coordination only. Among the other lithium titanate polymorphs, both the hexagonal and rocksalt structures have lithium ions residing only in octahedral voids. However, the SAED pattern of lithium titanate phase (Figure 2d) clearly indicates the presence of a cubic structure, so we can assign the $Li_{0.88}TiO_2$ to rocksalt type structure. This means, with high lithium concentration ($x \sim 0.9$), the lithium titanate prefers to adopt the rocksalt structure rather than the spinel type structure. This phase transition from spinel to rocksalt upon lithium insertion is consistent with X-ray absorption and diffraction spectroscopy[48] as well as computational results.[20]

From the analyses of the ^{6}Li NMR of lithium inserted TiO_2, it is clear that for increasing lithium concentrations there is a strong preference for the lithium titanate (Li_xTiO_2) structure over the rutile phase. The two Li-ion environments associated with Li in the rutile lattice (peak A) and Li in the rocksalt type lithium titanate lattice (peak C) have a striking difference in resonance width ($\Delta\nu$) as can be seen in Figure 3 and Table 1. Especially considering the fact that lithium is in an octahedral void in both the rutile and rocksalt lithium titanate structures, the origin of the line width needs further investigation. Under MAS (10 kHz) conditions the dipolar interactions and chemical shift anisotropy can be considered to have no contribution to the line width. Similarly, the quadrupolar interactions of ^{6}Li must be negligible due to the extremely small quadrupolar moment and high magnetic field (21.1 T) used in the present study. Therefore, we need to consider the distribution of isotropic chemical shifts (δ_{iso}) and coupling mechanisms with electrons.

There are two possible coupling mechanisms with electrons that could result in broad ^{6}Li resonance, namely, paramagnetic interactions and Knight shift interactions. Upon lithium insertion, an electron is donated to the host TiO_2 network, and if the electron becomes localized on Ti^{3+}, the atom can develop a paramagnetic moment. Even a very low concentration of Ti^{3+} paramagnetic ions can lead to paramagnetic interaction and effectively reduce the ^{6}Li spin$-$lattice relaxation (T_1) to as low as 10^{-4} s. However in the present study, the ^{6}Li spin$-$lattice relaxation (T_1) times of all the phases are on the order of 60 s (see Table 1). This clearly rules out the presence of any localized electron leading to Ti^{3+} and paramagnetic interactions in both the parent rutile and lithium titanate structures. The next coupling mechanism involves interactions with electrons in the conduction band, often referred as the Knight shift. During this interaction, the electron density in the conduction band has profound effects on the chemical shift and leads to a larger chemical shift typically in the range 100 ppm. However, a weak coupling to conduction electron could result in much smaller chemical shift, for example, Luca et al. reported the Knight shift of ^{6}Li NMR resonance for spinel type lithium titanate around -4 ppm.[26] In the present study the ^{6}Li chemical shift of all samples lies between $+1$ ppm to -1 ppm, which implies that conduction band electron coupling mechanism is not a major contributor to the observed line width for $Li_{0.88}TiO_2$ (peak C). Having ruled out the electron coupling mechanism, another possible origin for the line broadening is the distribution of isotropic chemical shifts (δ_{iso}), which generally arises due to amorphous and/or highly disordered environments. The X-ray diffraction patterns of lithium titanate phase (Figure 1d) are sharp and well-defined, which clearly indicates better crystallinity among lithium titanate crystallites. Further, the SAED studies reveal good crystalline nature of lithium titanate crystallites. Hence, the observed line width most likely originates from local structural distortion in the lithium titanate phase. The line width of rocksalt lithium titanate, i.e., $Li_{0.88}TiO_2$ (peak C), is about 220 Hz and covers the chemical shift ranging from -1 to $+1$ ppm. The ^{6}Li chemical shift correlation suggests $Li_{0.88}TiO_2$ has a wide range of lithium coordination environments with the major components being LiO_5 and LiO_6. In $LiTiO_2$ with the ordered structure, lithium occupies octahedral voids (16*c*) in a nearly ideal cubic close-packed oxygen array where lithium possesses 6-fold coordination.[24] On the other hand, the disordered rocksalt $LiTiO_2$ consists of a random distribution of titanium and lithium in the octahedral voids (16*c* and 16*d*) with an fcc oxygen array.[38] This random distribution of Ti and Li atoms could cause a variety of nearest neighbors for each lithium octahedron resulting in a range of Li$-$O bond lengths (see Figure 4d) and hence a distribution of isotropic chemical shifts in ^{6}Li NMR resonance. Considering the broad nature of the ^{6}Li line widths, we can confidently suggest $Li_{0.88}TiO_2$ has a disordered rocksalt structure. This type of disordered rocksalt

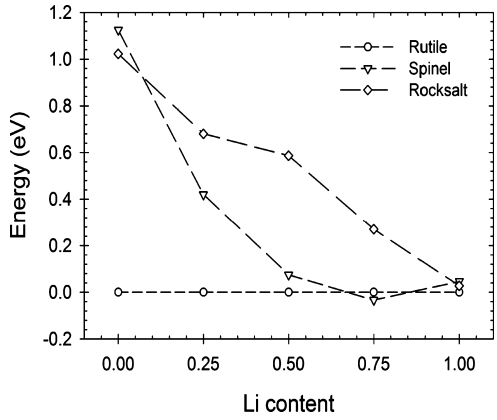

Figure 5. Total energy per TiO_2 unit obtained from the DFT calculations for the rutile (circle), spinel (triangle), and rocksalt (diamond) structures as a function of lithium content.

structure has been observed in lithium inserted titanium oxide and also in other transition metal oxides.[49]

DFT. The results presented above suggest the occurrence of two consecutive phase transitions during lithium insertion in rutile nanorods. Up to lithium fractions of $x = 0.12$ (see Table 1 and the discussion above), lithium is accommodated in nanostructured rutile without a significant change in the parent structure. Further lithium insertion ($x \sim 0.5$) leads to a structural phase transition from the tetragonal rutile structure to the cubic spinel structure. At lithium fractions of about $x \sim 0.9$, the spinel structure transforms into a disordered rocksalt structure. The three structures along with the disordered rocksalt structure predicted from ^{6}Li MAS NMR are schematically shown in Figure 4. In this section, we aim to validate the occurrence of the three different crystal structures upon lithium insertion in rutile on energetics grounds by carrying out DFT calculations. The DFT calculations are for bulk phases. Although simulations of nanoparticles immersed in an aqueous solution would be required for a direct comparison with experiment, we considered a much simpler and computationally accessible system (i.e., bulk phases) as a first step toward addressing the phase transformations of interest. In addition, this approach will enable us to separate the bulk driving force from the nanosizing effects. Figure 5 shows the total energy per TiO_2 unit of each of the three polymorphs as a function of Li content. For each value of x, the total energy is expressed relative to that of rutile at that same value of x. At low Li contents ($x \leq 0.25$), there is a large energetic difference between the rutile and lithium titanate phases (i.e., the spinel and rocksalt structures). Because of this greater stability of rutile, the parent structure is expected to retain its original tetragonal structure, without significant modifications, at lower lithium insertion levels ($x \leq 0.25$). This is clearly seen in the present study where for the lithium concentration of $x = 0.12$ (i.e., $Li_{0.12}TiO_2$) the nanostructured TiO_2 retains its original rutile structure. In addition, the DFT results indicate that, as the Li content increases ($x > 0.25$), the difference in energy between the three polymorphs decreases sharply (see Figure 5). At a Li content of $x = 0.50$ per TiO_2 unit, the spinel and rutile polymorphs are essentially energetically equivalent; hence a phase transformation from rutile to spinel is possible on energetics grounds at this lithium concentration. In our experimental study discussed earlier the lithium titanate phase with lithium concentration of $x = 0.46$ (i.e., $Li_{0.46}TiO_2$) was found to adopt the spinel structure, in good agreement with the DFT calculations. This phase transition from rutile to spinel requires extensive rearrangement of TiO_6 octahedra and causes a unit cell volume change of 5.6%.[50] The DFT calculations show that further lithiation ($x > 0.50$) of the spinel lithium titanate leads to displacement of the lithium ions from the tetrahedral (8*a*) to the octahedral sites (16*c*), which are vacant in the spinel structure. At the Li content of $x \sim 0.75$, the Li ions are distributed between tetrahedral and octahedral sites, and as the Li content increases further to $x = 1$, Li ions occupy only octahedral sites in the spinel structure leading to a rocksalt type phase. This result agrees quite well with neutron diffraction experiments by Cava et al.[24] and the first-principles calculations of Koudriachova et al.[51] Our DFT calculations further predict that all three structures, i.e., rutile, spinel and rocksalt structures, become energetically equivalent for lithium concentration of $x \approx 1$, which is in good agreement with the formation of a rocksalt structure for lithium concentration of $x = 0.88$ (i.e., $Li_{0.88}TiO_2$) in the present study. It is noteworthy that the phase transformation from spinel to rocksalt requires neither extensive structural rearrangement nor significant volume change.[50] At $x = 1.0$, the spinel and rocksalt polymorphs only differ by their arrangement of Li and Ti ions in the octahedral site. The DFT-predicted lattice parameters for the spinel and rocksalt phases are consistent with this statement. Indeed, the spinel lattice parameters were calculated to be 8.634 and 8.641 Å at $x = 0.5$ and 1.0, respectively, and the disordered rocksalt lattice parameter, estimated from averaging the three lattice lengths of the ordered rocksalt (which showed a slight anisotropy due to its ordered structure with alternating LiO_2 and TiO_2 layers) was 8.475 Å.

Conclusion

The high field ^{6}Li MAS NMR combined with DFT study is utilized to study the structural evolution during chemical lithium insertion into rutile nanorods. The host rutile nanorod holds lithium insertion only up to $0.12Li/TiO_2$ (i.e., $x = 0.12$) without significant changes in either nanorod morphology or structure. The ^{6}Li MAS NMR study shows that during lithium insertion rutile nanorod accommodates lithium in off-centered octahedral. Further lithium insertion ($x \sim 0.5$) induces a structural transition from rutile to spinel type structure ($Li_{0.44}TiO_2$) where lithium resides in tetrahedral position as revealed by ^{6}Li MAS NMR. Our DFT studies reveal that at this lithium concentration a spinel type structure has similar energy requirements as of rutile, which corroborate our experimental studies. In previous reports,[10,22] this intermediate spinel type phase has not been observed, mainly because the XRD pattern used to study the phase transition is insensitive to differentiating the rock salt and spinel phase of nanocrystallite particles. In contrast, in the present study using XRD combined with high field ^{6}Li MAS NMR, we were able to indentify this intermediate phase as spinel type structure. This phase transition (from rutile $P4_2/mnm$ to spinel $Fd\bar{3}m$) is responsible for plateau region at 1.4 V observed in discharge profile of rutile electrodes.[9,10] This phase transition is accompanied by volume changes of about 6% and extensive rearrangement of the TiO_6 octahedra. The change in unit cell volume due to lithium insertion causes abundant strains on the original nanostructured rutile crystallites and may explain the large irreversible capacity loss of rutile observed in the first lithium insertion/deinsertion during cycling experiments. Further lithium insertion ($x \sim 0.9$) leads to a second phase transition to rocksalt type structure ($Fm\bar{3}m$). Our DFT study indicates a low energy requirement for the formation of rocksalt type structure at this lithium concentration ($x \sim 0.9$) and supports the possible phase transition from spinel to rocksalt type lithium titanate phase. Further it reveals that during this phase transition lithium ions in tetrahedral holes of spinel structures are displaced to octahedral environments leading to rocksalt type structure. This

lithium displacement from tetrahedral to octahedral voids accompanied with phase transition is clearly observed in our high field ^{6}Li MAS NMR chemical shift analysis. This structural transition requires neither extensive rearrangement of the TiO_6 network nor unit cell volume changes (<1.6%), and hence this phase transition will not affect electrochemical cycling and expected to give stable capacity. The careful analysis of ^{6}Li MAS NMR line width of this rocksalt phase reveals a disordered type structure with possibility of random distribution of lithium and titanium in octahedral voids. It is noteworthy that similar phase transition is also found in our ongoing study of chemical insertion into anatase nanoparticles, which will be published separately. This structural transition during lithium insertion of TiO_2 could cause battery degradation during electrochemical cycles, hence fully phase transformed lithium titanate might provide more stable reversible capacity.

Acknowledgment. This work is supported by the Laboratory-Directed Research and Development Program (LDRD) of the Pacific Northwest National Laboratory (PNNL) and by the Office of Basic Energy Sciences (BES), U.S. Department of Energy (DOE). The TEM & NMR work was carried out at the Environmental and Molecular Science Laboratory, a national scientific user facility sponsored by the DOE's Office of Biological and Environmental Research (BER). PNNL is a multiprogram laboratory operated by Battelle Memorial Institute for the Department of Energy under Contract DE-AC05-76RL01830. We thank Dr. Robert Heck for his help in editorial suggestions and corrections.

References and Notes

(1) Martin Winter, J. O. B.; Spahr, M. E.; Novák, P. *Adv. Mater.* **1999**, *10*, 725.
(2) Whittingham, M. S. *Chem. Rev.* **2004**, *104*, 4271.
(3) Yang, Z.; Choi, D.; Kerisit, S.; Rosso, K. M.; Wang, D.; Zhang, J.; Graff, G.; Liu, J. *J. Power Sources*, in press.
(4) Zachau-Christiansen, B.; West, K.; Jacobsen, T.; Atlung, S. *Solid State Ionics* **1988**, *28*−*30*, 1176.
(5) Arico, A. S.; Bruce, P.; Scrosati, B.; Tarascon, J.-M.; van Schalkwijk, W. *Nat. Mater.* **2005**, *4*, 366.
(6) P. Poizot, S. L.; Grugeon, S.; Dupont, L.; Tarascon, J.-M. *Nature* **2000**, *407*, 496.
(7) Kim, J.; Cho, J. *J. Electrochem. Soc.* **2007**, *154*, A542.
(8) Wagemaker, M.; Borghols, W. J. H.; Mulder, F. M. *J. Am. Chem. Soc.* **2007**, *129*, 4323.
(9) Macklin, W. J.; Neat, R. J. *Solid State Ionics* **1992**, *53*−*56*, 694.
(10) Hu, Y.-S.; Kienle, L.; Guo, Y.-G.; Maier, J. *Adv. Mater.* **2006**, *18*, 1421.
(11) Sodergren, S.; Siegbahn, H.; Rensmo, H.; Lindstrom, H.; Hagfeldt, A.; Lindquist, S.-E. *J. Phys. Chem. B* **1997**, *101*, 3087.
(12) Li, J.; Tang, Z.; Zhang, Z. *Electrochem. Solid-State Lett.* **2005**, *8*, A316.
(13) Armstrong, A. R.; Armstrong, G.; Canales, J.; Bruce, P. G. *J. Power Sources* **2005**, *146*, 501.
(14) Jiang, C.; Honma, I.; Kudo, T.; Zhou, H. *Electrochem. Solid-State Lett.* **2007**, *10*, A127.
(15) Borghols, W. J. H.; Wagemaker, M.; Lafont, U.; Kelder, E. M.; Mulder, F. M. *Chem. Mater.* **2008**, *20*, 2949.
(16) Reddy, M. A.; Kishore, M. S.; Pralong, V.; Caignaert, V.; Varadaraju, U. V.; Raveau, B. *Electrochem. Commun.* **2006**, *8*, 1299.
(17) Lindstrom, H.; Sodergren, S.; Solbrand, A.; Rensmo, H.; Hjelm, J.; Hagfeldt, A.; Lindquist, S.-E. *J. Phys. Chem. B* **1997**, *101*, 7717.
(18) Henningsson, A.; Rensmo, H.; Sandell, A.; Siegbahn, H.; Sodergren, S.; Lindstrom, H.; Hagfeldt, A. *J. Chem. Phys.* **2003**, *118*, 5607.
(19) Stashans, A.; Lunell, S.; Bergström, R.; Hagfeldt, A.; Lindquist, S.-E. *Phys. Rev. B* **1996**, *53*, 159.
(20) Tielens, F.; Calatayud, M.; Beltrán, A.; Minot, C.; Andrés, J. *J. Electroanal. Chem.* **2005**, *581*, 216.
(21) Koudriachova, M. V.; Harrison, N. M.; de Leeuw, S. W. *Comput. Mater. Sci.* **2002**, *24*, 235.
(22) Baudrin, E.; Cassaignon, S.; Koelsch, M.; Jolivet, J. P.; Dupont, L.; Tarascon, J. M. *Electrochem. Commun.* **2007**, *9*, 337.
(23) Koudriachova, M. V.; de Leeuw, S. W.; Harrison, N. M. *Chem. Phys. Lett.* **2003**, *371*, 150.
(24) Cava, R.J. D. W. M.; Zahurak, S.; Santoro, A.; Roth, R. S. *J. Solid State Chem.* **1984**, *53*, 64.
(25) Armstrong, A. R.; Paterson, A. J.; Dupre, N.; Grey, C. P.; Bruce, P. G. *Chem. Mater.* **2007**, *19*, 1016.
(26) Luca, V.; Hanley, T. L.; Roberts, N. K.; Howe, R. F. *Chem. Mater.* **1999**, *11*, 2089.
(27) Krtil, P.; Dedecek, J.; Kostlanova, T.; Brus, J. *Electrochem. Solid-State Lett.* **2004**, *7*, A163.
(28) Massiot, D.; Fayon, F.; Capron, M.; King, I.; Le Calvé, S.; Alonso, B.; Durand, J. O.; Bujoli, B.; Gan, Z.; Hoatson, G. *Magn. Reson. Chem.* **2002**, *40*, 70.
(29) Dovesi, R.; Saunders, V. R.; Roetti, C.; Orlando, R.; Zicovish-Wilson, C. M.; Pascale, F.; Civalleri, B.; Doll, K.; Harrison, N. M.; Bush, I.; D'Arco, P.; Llunell, M. *CRYSTAL06 User's Manual*; University of Torino: Torino, 2006.
(30) Zicovish-Wilson, C. M. LOptCG; Valencia, Spain, 1998.
(31) Catti, M.; Valerio, G.; Dovesi, R. *Phys. Rev. B* **1995**, *51*, 7441.
(32) Apra, E. Ph.D. Thesis, University of Torino, 1992.
(33) Durand, P.; Barthelat, J. C. *Theor. Chim. Acta* **1975**, *38*, 283.
(34) Hull, S.; Farley, T. W. D.; Hayes, W.; Hutchings, M. T. *J. Nucl. Mater.* **1988**, *160*, 125.
(35) Dovesi, R.; Roetti, C.; Freyria-Fava, C.; Prencipe, M.; Saunders, V. R. *Chem. Phys.* **1991**, *156*, 11.
(36) Abrahams, S. C.; Bernstein, J. L. *J. Chem. Phys.* **1971**, *55*, 3206.
(37) Cava, R. J.; Murphy, D. W.; Zahurak, S.; Santoro, A.; Roth, R. S. *J. Solid State Chem.* **1984**, *53*, 64.
(38) Lecerf, A. *Ann. Chim.* **1962**, *7*, 513.
(39) Thackeray, M. *J. Am. Ceram. Soc.* **1999**, *82*, 3347.
(40) Wang, D.; Choi, D.; Yang, Z.; Viswanathan, V. V.; Nie, Z.; Wang, C.; Song, Y.; Zhang, J.-G.; Liu, J. *Chem. Mater.* **2008**, *20*, 3435.
(41) Bond, S. P.; Gelder, A.; Homer, J.; McWhinnie, W. R.; Perry, M. C. *J. Mater. Chem.* **1991**, *1*, 327.
(42) Xu, Z.; Stebbins, J. F. *Solid State Nucl. Magn. Reson.* **1995**, *5*, 103.
(43) Koudriachova, M. V.; Harrison, N. M.; de Leeuw, S. W. *Solid State Ionics* **2003**, *157*, 35.
(44) Alam, T. M.; Conzone, S.; Brow, R. K.; Boyle, T. J. *J. Non-Cryst. Solids* **1999**, *258*, 140.
(45) Koudriachova, M. V.; Harrison, N. M.; de Leeuw, S. W. *Phys. Rev. B* **2002**, *65*, 235423.
(46) Akimoto, J.; Gotoh, Y.; Sohma, M.; Kawaguchi, K.; Oosawa, Y.; Takei, H. *J. Solid State Chem.* **1994**, *110*, 150.
(47) Wagemaker, M.; Kearley, G. J.; van Well, A. A.; Mutka, H.; Mulder, F. M. *J. Am. Chem. Soc.* **2003**, *125*, 840.
(48) Ra, W.; Nakayama, M.; Uchimoto, Y.; Wakihara, M. *J. Phys. Chem. B* **2005**, *109*, 1130.
(49) Hewston, T. A.; Chamberland, B. L. *J. Phys. Chem. Solids* **1987**, *48*, 97.
(50) Murphy, D. W.; Cava, R. J.; Zahurak, S. M.; Santoro, A. *Solid State Ionics* **1983**, *9*−*10*, 413.
(51) Koudriachova, M. V. *Phys. Chem. Chem. Phys.* **2008**, *10*, 5094.

JP904148Z